Environmental Science
Water Research & Technology

PAPER

View Article Online
View Journal | View Issue

Cite this: *Environ. Sci.: Water Res. Technol.*, 2018, **4**, 1282

Degradation of 1*H*-benzotriazole by UV/H_2O_2 and UV/TiO_2: kinetics, mechanisms, products and toxicology†

Ya Chen, Jinshao Ye, Chongshu Li, Pulin Zhou, Juan Liu and Huase Ou *

Received 23rd February 2018,
Accepted 21st April 2018

DOI: 10.1039/c8ew00116b

rsc.li/es-water

Benzotriazoles are emerging contaminants widespread in environmental waters. As they are robust against conventional biological wastewater treatment, it is desirable to develop cost-effective and safe treatment methods for benzotriazole removal. The current study attempted to investigate the degradation of water dissolved 1*H*-benzotriazole (1H-BTA) with UV/H_2O_2 and UV/TiO_2. Pseudo-first order degradation kinetics were observed in low power 280 nm UV/H_2O_2 and UV/TiO_2 systems (UV intensity = 0.023 mW cm^{-2}, k_{app} reached 1.63×10^{-3} s^{-1} and 1.87×10^{-3} s^{-1}, respectively), and radical oxidation was the dominant reaction mechanism with $k_{\cdot OH\text{-}BTA}$ at $(7.1 \pm 0.8) \times 10^9$ M^{-1} s^{-1} and $(6.9 \pm 0.7) \times 10^9$ M^{-1} s^{-1}. Both systems were affected by the pH value, natural organic matter and anions, leading to incomplete mineralization in actual water treatment processes. As the reaction proceeded, 1H-BTA was progressively transformed into eight organic products. The number of preliminary hydroxylated products (*e.g.* $C_6H_5N_3O$) increased rapidly at the early stage, while the further open-loop products (*e.g.* $C_4H_3N_3O_4$) were dominant at the later stage. Based on the proteomics analysis, the significant activation of ribosome, transporter and tricarboxylic acid cycle metabolisms in *Escherichia coli*, which exposed to the later degradation product mixture, suggested that the toxicity of 1H-BTA decreased. In conclusion, incomplete mineralization using hydroxyl radical oxidation likewise has potential for thedetoxification of 1H-BTA.

Water impact

This study provides insights into the generation mechanism, pathways and toxicity variation of the degradation products of 1*H*-benzotriazole (1H-BTA) in hydroxyl radical oxidation, clarifying that the incomplete mineralization of 1H-BTA is effective for its detoxification. We study the contribution of the photocatalytic degradation of organic matter and the effects of their degradation products on the fundamental physiological processes in model microorganisms.

1. Introduction

Benzotriazoles (BTAs) are widely applied as additive agents to prevent yellowing and degradation of a variety of industrial products, such as building materials, automobile components, paints, adhesive agents, films, shoes, glasses and tires.[1] In recent years, they have been considered as a kind of emerging contaminant due to persistence, bioaccumulative ability and toxicity.[2,3] The annual output of BTAs reaches 9000 tons worldwide,[4] and some are released into the environment through human activity. The most common BTA, 1*H*-benzotriazole (1H-BTA), was one of the few compounds that was present in tap water and recycled water,[5,6] even in the finished water of an advanced wastewater recycling facility using reverse osmosis and ultraviolet irradiation.[7] As the final step of the anthropogenic water cycle, wastewater treatment plants (WWTPs) receive undesired contaminants, *e.g.* BTAs. Removal efficiencies of different BTAs in conventional WWTPs varied from 13% to 74%;[8] the robustness of BTAs against conventional biological wastewater treatments increases their undesired occurrence in natural water bodies.[4] Therefore, it is desirable to develop cost-effective treatment methods to remove BTAs.

Degradation of BTAs in an aqueous matrix was explored with a variety of advanced oxidation processes (AOPs), such as ozonation, photochemical oxidation, electrochemical oxidation and ultrasonication.[9–13] Among these methods, ultraviolet driven AOPs (UV-AOPs), especially UV/H_2O_2 and UV/TiO_2 photocatalysis, have shown great potential as low-cost, environmentally-friendly and sustainable treatment technologies. There are only a few studies dealing with the application of UV-AOPs for BTA elimination. The main oxidizing species in both UV/H_2O_2 and UV/TiO_2 photocatalysis has been

School of Environment, Guangdong Key Laboratory of Environmental Pollution and Health, Jinan University, Guangzhou 510632, China.
E-mail: touhuase@jnu.edu.cn; Fax: +86 20 85226615; Tel: +86 20 85226615

† Electronic supplementary information (ESI) available. See DOI: 10.1039/c8ew00116b

confirmed to be a hydroxyl radical (˙OH; E^0 = 1.80–2.70 V), which induces non-selective oxidation of BTAs.[14] The degradation of basic monomer 1H-BTA using UV/H_2O_2 was confirmed to be a pseudo-first order reaction,[12] and had a higher efficiency than using ozonation.[13] Several novel photocatalytic materials were synthesized to increase the degradation efficiency of BTAs.[10,15] However, there is still a knowledge gap with respect to the detailed mechanisms and pathways in the degradation of BTAs using ˙OH oxidation, not to mention the systematic evaluation of the residual toxicity of degradation products.

In actual water treatment processes, a full mineralization of targeted organic contaminants will expend a large amount of energy and chemical materials. Other coexisting contaminants *e.g.*, natural organic matter (NOM), anions and particulate matter, may become potential competitors in consuming ˙OH.[16] Incomplete mineralization is ubiquitous in UV-AOP applications for targeted contaminant (*e.g.*, BTAs) elimination. Therefore, a comprehensive toxicological assessment of BTAs and their degradation products is essential. Interactions between BTAs (or products) and organisms involve a series of molecular mechanisms of action with fundamental physiological processes. The related exploration deep into protein expression and metabolic pathways will reveal unknown negative effects of BTAs (or products) on organisms; it will further be informative to systematically evaluate the residual or newly generated toxicity of degradation products. So far, the existing toxicological evaluation of BTAs and their degradation products is still limited to several traditional techniques based on the phenotype changes of specific model organisms.[12,17]

The present study was designed to examine the efficacies of the degradation of 1H-BTA by UV/H_2O_2 and UV/TiO_2 treatments. A high resolution mass spectrometer (HRMS) was used to tentatively identify the degradation products of 1H-BTA, followed by the speculation of degradation mechanisms and pathways. The biological effects of the degradation product mixture on fundamental protein expression and metabolic networks were evaluated with a quantitative proteomic technology.

2. Materials and methods

2.1. Materials

Degussa P25 TiO_2 (nanopowder, 21 nm primary particle size, ≥99.5%), 1H-BTA (99%, HPLC grade), ethyl alcohol (EtOH, HPLC grade), *tert*-butyl alcohol (TBA, HPLC grade), humic acid (HA) (90% dissolved organic matter, CAS: 1415-93-6) and isobaric tags for relative and absolute quantitation (iTRAQ) reagent multiplex kits (PN 4352135) were purchased from Sigma-Aldrich (USA). Analytical grade H_2O_2 (30%, v/v), $NaNO_3$ (98%), NaCl (98%) and humic acid (90%) were purchased from Sinopharm (China). Other chemical reagents were prepared using the highest purity available (Text S1 of the ESI;† "S" designates texts, tables, figures and other content in the ESI† hereafter). All of the solutions were prepared using ultrapure water (18.2 MΩ) produced by a Milli-Q Advantage A10 system (Millipore, USA).

2.2. Ultraviolet irradiation module and degradation

A new UVLED module, consisting of a 280 nm UVLED light source, framework and reactor vessel, was designed and assembled as an improved version of our previous module (Fig. S1†).[18] The irradiation intensity was 0.023 mW cm^{-2} on the surface of the solution matrix. Before reaction, 20 mL of 1H-BTA solution ($[1H\text{-}BTA]_0$ = 8.39 μM) were spiked into the reactor vessel. The initial concentrations of H_2O_2 and TiO_2 were 4.41 mM and 2.50 mM in UV/H_2O_2 and UV/TiO_2 experiments, respectively. The solution was maintained at 25 ± 2 °C and pH = 6.8–7.2 (if not specified otherwise), and the dish was shaken at 60 rpm. At a pre-set time, ascorbic acid was added to scavenge H_2O_2. For UV/TiO_2 experiments, all acquired samples were filtered with a 0.22 μm polyether sulfone filter to remove TiO_2. Control experiments using water, H_2O_2 and TiO_2 were also performed. The pH value was adjusted using a pH buffered solution, which contained different concentration combinations of NaOH, KH_2PO_4 and H_3PO_4. For experiments examining the influence factors, a predetermined amount of $NaNO_3$, NaCl or humic acid was added. For the radical species identification experiment, EtOH and TBA were used to probe the formation of ˙OH. Each time a single probe (100 mM) was added. All the obtained samples were transferred to brown amber tubes (stored at 4 °C) before analysis.

2.3. Molar absorption coefficient, quantum yield and competition kinetics

Molar absorption (extinction) coefficients (ε) of various solutions (1H-BTA, scavengers and anions) were obtained based on the absorbance (range from 200 nm to 300 nm) with a Chirascan circular dichroism spectrometer (Applied Photophysics, UK). The measurements were conducted under N_2 purging to avoid the optical absorption by O_2. Cuvettes with various light path lengths (0.1 and 1.0 cm) were used to ensure accuracy. Quantum yields of 1H-BTA were calculated following a similar procedure developed by Duca *et al.*[19]

The second-order rate constant for the reaction of 1H-BTA (T) with ˙OH was determined by competition kinetics in a binary mixture with *para*-chlorobenzoic acid (*p*CBA) as a reference compound (R).[20] Based on the ˙OH reaction rate constant with the reference compounds (k_R), the ˙OH reaction rate constant with 1H-BTA (k_T) can be determined based on eqn (1).[21]

$$\ln\left(\frac{[T]}{[T]_0}\right) = \frac{k_T}{k_R}\ln\left(\frac{[R]}{[R]_0}\right) \quad (1)$$

2.4. Measurement of 1*H*-benzotriazole and degradation products

Degradation products were identified with a TripleTOF 5600+ HRMS (Applied Biosystems SCIEX). Quantification of 1H-BTA

and its degradation products was performed with a TripleQuad 5500 tandem mass spectrometer (Applied Biosystems SCIEX). The detailed analysis procedures are presented in Text S2, and Tables S1 and S2.† Furthermore, total organic carbon (TOC) was measured with a LiquidTOC Trace analyzer (Elementar). The product analysis procedure here meets level 3, namely tentative candidates, in the Schymanski framework.[22]

2.5. Proteomics analysis

Proteomics analysis includes four steps: (1) cell exposure to the target contaminants; (2) protein digestion; (3) peptides labeled using iTRAQ and (4) peptide analysis using a TripleTOF 5600+ HRMS equipped with a Nanospray III source and a NanoLC 400 system (Applied Biosystems SCIEX). Samples of target contaminants include: (1) 60 mL 8.39 μM 1H-BTA solution; (2) 60 mL UV/H_2O_2 treated sample (UV/H_2O_2 degradation product mixture) and (3) 60 mL UV/TiO_2 treated sample (UV/TiO_2 degradation product mixture). The reaction conditions were as follows: temperature = 25 ± 2 °C, pH = 6.5–7.2, $[1H\text{-}BTA]_0$ = 8.39 μM, $[H_2O_2]_0$ = 4.41 mM, $[TiO_2]_0$ = 2.50 mM and reaction time = 30 min. *Escherichia coli* ATCC11303 was selected as the model microorganism, and was inoculated at 100 r min^{-1} for 12 h. The *E. coli* cells were obtained by centrifugation at 3500 × *g* for 10 min and were washed three times. In the exposure stage, the cells (0.1 g L^{-1}) were inoculated in the dark at 25 °C for 24 h using a 20 mL medium, which contained 30 mg L^{-1} KH_2PO_4, 70 mg L^{-1} NaCl, 30 mg L^{-1} NH_4Cl, 10 mg L^{-1} $MgSO_4$, 30 mg L^{-1} beef extract, 100 mg L^{-1} peptone and 1 mg L^{-1} 1H-BTA or its degradation product mixture. The exposed cells were separated and washed with a phosphate buffer solution before protein extraction. The following protein digestion, iTRAQ labeling and HRMS analysis followed the same procedures described in our previous study.[23]

2.6. Degradation experiments with field water samples

Field water samples were collected from two different drinking water treatment plants (DWTP) in Guangzhou, China. The main treatment processes include pre-chlorination, coagulation (using poly aluminium chloride), sedimentation, filtration and disinfection (using liquid chlorine). The source water (from the Pearl River) and finished water of these two DWTPs were obtained, and the analysis methods of water parameters are presented in Text S3.† The degradation experiments of 1H-BTA were conducted using these four different actual water bodies as background matrices. The initial concentration of 1H-BTA was 8.39 μM, with 4.41 mM H_2O_2 and 2.50 mM TiO_2 added into the reaction systems.

3. Results and discussion

3.1. Degradation efficiency and mechanism

Because 1H-BTA is stable under UVA and UVB irradiation,[24] only UVC (280 nm UVLED) was applied in the present study. Negligible variation of 1H-BTA concentration was observed in sole water, H_2O_2 and TiO_2 control experiments (Fig. 1a), indicating that 1H-BTA was not directly removed by H_2O_2 oxidation or TiO_2 adsorption. Approximately 10% of 1H-BTA was removed with 30 min 0.023 mW cm^{-2} UV-C irradiation at 280 nm. The photolysis of 1H-BTA followed a first order reaction kinetics with a rate constant ($k_{280\ nm}$) of 0.04 × 10^{-3} s^{-1} (Fig. 1b), which was obviously lower than that in the experiment using high-power (100 W) UV irradiation.[12] After 30 min UV/H_2O_2 and UV/TiO_2 reactions, the removal efficiency of 1H-BTA (8.39 μM) reached 95% and 97%, respectively (Fig. 1b and c). These degradation processes followed a pseudo-first order kinetic model with apparent rate constants (k_{app}) of 1.63 × 10^{-3} s^{-1} (half-life $t_{0.5}$ = 7.09 min) and 1.87 × 10^{-3} s^{-1} ($t_{0.5}$ = 6.18 min), respectively. The improvement after using these two treatments can be attributed to $^{\cdot}OH$ oxidation observed by scavenging studies (detailed information is presented in Text S4†).

Fig. 1d shows the variation of TOC. For the 8.39 μM 1H-BTA solution, the apparent TOC value was ~0.60 mg L^{-1} at time zero. After 30 min reaction, nearly 72% (UV/H_2O_2) or 60% (UV/TiO_2) of TOC was removed, *i.e.*, the mineralization rate was higher with UV/H_2O_2 than with UV/TiO_2 under similar 1H-BTA removal rates (>95%). These TOC results indicated incomplete degradation of 1H-BTA in both reactions, probably due to the low power of UVLED light sources. Incomplete mineralization also implied the generation of various degradation products.

3.2. Degradation kinetics

Two mechanisms, including 280 nm photolysis and $^{\cdot}OH$ oxidation, reveal the degradation of 1H-BTA synchronously. Thus, the reaction rate of 1H-BTA in UV/H_2O_2 and UV/TiO_2 systems can be calculated by:

$$-\frac{d[1H\text{-}BTA]}{dt} = \left(k_{280nm} + k_{OH\text{-}BTA} \times [^{\cdot}OH]\right) \times [1H\text{-}BTA] = k_{app} \times [1H\text{-}BTA] \quad (2)$$

Determining these reaction rate constants will further verify the reaction mechanisms, as well as provide basic kinetics information.

Kinetics of the 280 nm irradiation can be deduced from the sole UV-C system. In the current sole UV-C (0.023 mW cm^{-2} at 280 nm) system, photolysis of 1H-BTA followed a first order reaction kinetics with a $k_{280\ nm}$ of 0.04 × 10^{-3} s^{-1} (Table 1). Using this $k_{280\ nm}$ as the reference, photolysis of 1H-BTA induced by 280 nm irradiation at the same intensity in UV/H_2O_2 and UV/TiO_2 systems followed a similar rate with a $k_{280\ nm}$ of 0.04 × 10^{-3} s^{-1}. Considering that the total apparent reaction rate constants for UV/H_2O_2 and UV/TiO_2 were 1.63 × 10^{-3} s^{-1} and 1.87 × 10^{-3} s^{-1}, which were significantly higher than $k_{280\ nm}$, this result reconfirmed that $^{\cdot}OH$ oxidation was the predominant degradation mechanism. The apparent quantum yield for 280 nm photolysis ($\Phi_{280\ nm}$) was

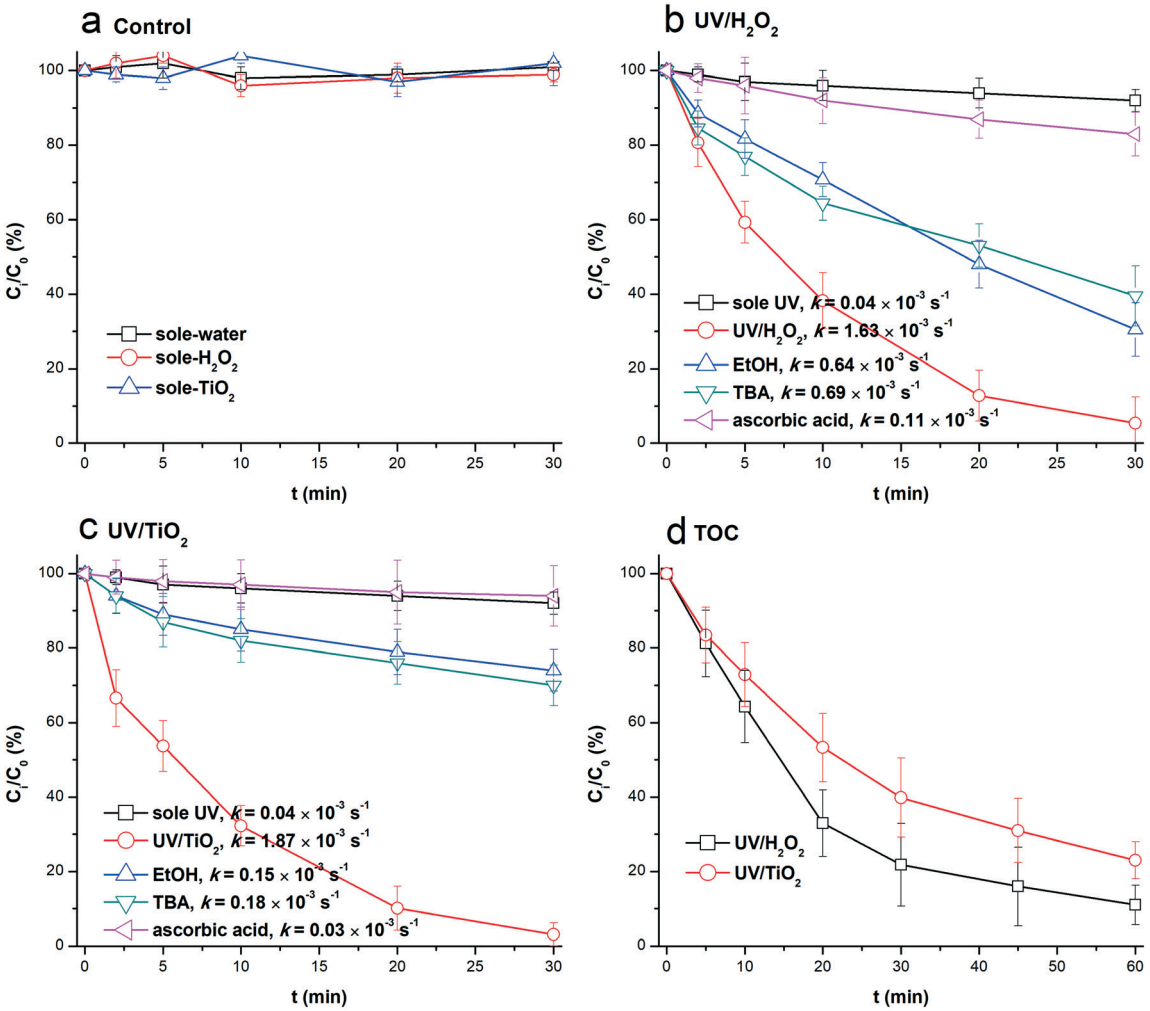

Fig. 1 Degradation of 1H-BTA with (a) the control, (b) UV/H_2O_2, (c) UV/TiO_2 and (d) variation of TOC.

Table 1 Kinetics parameters in UV/H_2O_2 and UV/TiO_2 systems

Sole UV		UV/H_2O_2			UV/TiO_2
$k_{280\ nm}$ (s^{-1})	$\Phi_{280\ nm}$	k_{app} (s^{-1})	$k_{\cdot OH\text{-}BTA}$ ($M^{-1}\ s^{-1}$)	$\Phi_{\cdot OH\text{-}BTA}$	k_{app} (s^{-1})
$(0.04 \pm 0.003) \times 10^{-4}$	0.002 ± 0.0002	$(1.63 \pm 0.23) \times 10^{-3}$	$(7.1 \pm 0.8) \times 10^{9}$	0.12 ± 0.02	$(1.87 \pm 0.20) \times 10^{-3}$

Experimental conditions: solution temperature 25 ± 2 °C, pH 6.5–7.2, $[1H\text{-}BTA]_0$ = 8.39 μM, 280 UV irradiation intensity = 0.023 mW cm^{-2}, $[H_2O_2]_0$ = 4.41 mM, $[TiO_2]_0$ = 2.50 mM.

further calculated to be 0.002 ± 0.0002,[19] indicating a low UV-C utilization ratio and the robustness of 1H-BTA.

Second-order rate constants ($k_{\cdot OH\text{-}BTA}$) between 1H-BTA and ·OH can be obtained based on a completed reaction with *p*CBA. Using a calculation procedure developed by Huber *et al.*,[21] $k_{\cdot OH\text{-}BTA}$ was $(7.1 \pm 0.8) \times 10^9$ M^{-1} s^{-1} in UV/H_2O_2 systems. Based on these obtained reaction constants, [·OH] was calculated to be ~1.73×10^{-13} M. The apparent quantum yield for these two systems ($\Phi_{\cdot OH\text{-}BTA}$, dominated by ·OH oxidation) was calculated to be 0.12 ± 0.02. Still, as the direct photolysis induced by 254 nm was ignored for the completed reaction calculation, the $k_{\cdot OH\text{-}BTA}$ obtained here was somewhat overestimated. Leitner *et al.*[13] reported a $k_{\cdot OH\text{-}BTA}$ of (1.07 ± 0.45) × 10^{10} M^{-1} s^{-1} in the UV/H_2O_2 system under pH = 6.25, and they used ibuprofen as the reference compound. In a more recent study, Borowska *et al.*[12] applied a specific calculation method but not a completed reaction to obtain the kinetic parameters in the UV/H_2O_2 system, and they calculated a $k_{\cdot OH\text{-}BTA}$ of 2.70×10^9 M^{-1} s^{-1} when pH = 7.0. These various $k_{\cdot OH\text{-}BTA}$ values can be attributed to the different experimental conditions, reference compounds or calculation methods.

3.3. Degradation products

Screening of potential degradation products from HRMS data was performed based on the possible transformation of 1H-

Table 2 Organic degradation products of 1H-BTA in UV/H_2O_2 and UV/TiO_2 treatments

Name	Product A	Product B	Product C	Product D	Evolution tendency in the UV/H_2O_2 system
Proposed structure	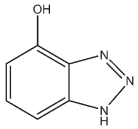	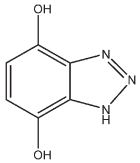	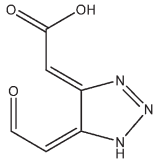	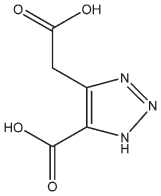	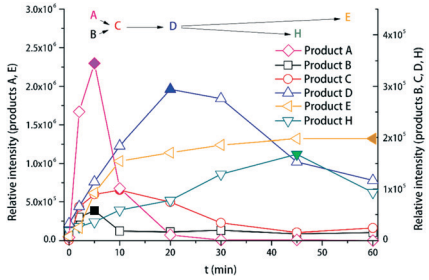
Molecular formula	$C_6H_5N_3O$	$C_6H_5N_3O_2$	$C_6H_5N_3O_3$	$C_5H_5N_3O_4$	
$[M + H]^+$: theoretical *m/z*	136.0505	152.0454	168.0404	172.0353	
$[M + H]^+$: observed *m/z*	136.0500	152.0454	168.0402	172.0349	
Retention time (min)	2.61	1.62	1.31	0.88	
Observed in reaction	UV/H_2O_2, UV/TiO_2	UV/H_2O_2, UV/TiO_2	UV/H_2O_2, UV/TiO_2	UV/H_2O_2, UV/TiO_2	
Extracted ion chromatography	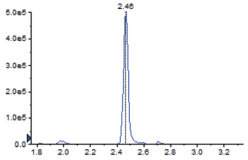	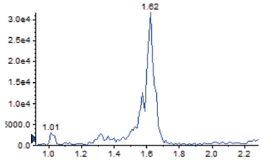	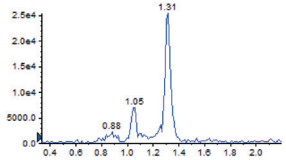	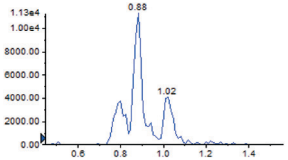	

Name	Product E	Product F	Product G	Product H	Evolution tendency in the UV/TiO_2 system
Proposed structure	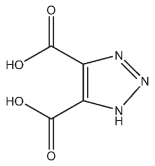	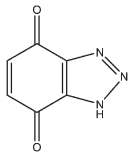	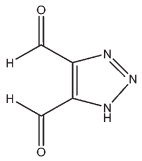	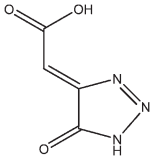	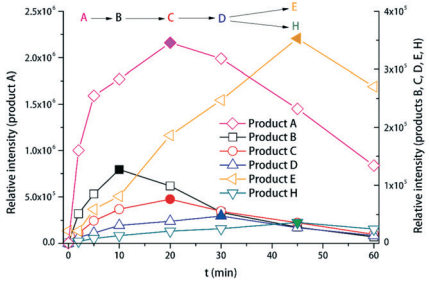
Molecular formula	$C_4H_3N_3O_4$	$C_6H_3N_3O_2$	$C_4H_3N_3O_2$	$C_4H_3N_3O_3$	
$[M + H]^+$: theoretical *m/z*	158.0196	150.0298	126.0298	142.0247	
$[M + H]^+$: observed *m/z*	158.0190	150.0297	126.0289	142.0243	
Retention time (min)	1.07	2.14	0.70	1.19	
Observed in reaction	UV/H_2O_2, UV/TiO_2	UV/TiO_2	UV/H_2O_2, UV/TiO_2	UV/H_2O_2, UV/TiO_2	
Extracted ion chromatography	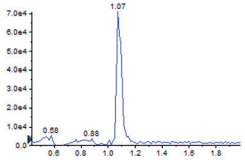	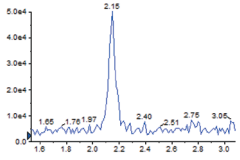	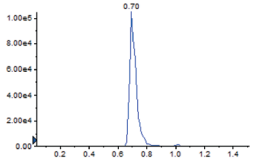	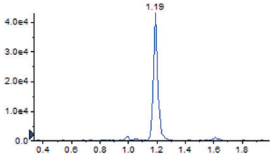	

Experimental conditions: solution temperature 25 ± 2 °C, pH 6.5–7.2, $[1H\text{-}BTA]_0$ = 0.84 μM, $[H_2O_2]_0$ = 44.12 μM, $[TiO_2]_0$ = 2.50 μM. More detailed information of other products is listed in the ESI.

BTA under $^{\cdot}OH$ attack. Eight potential stable products were proposed in the UV/H_2O_2 and UV/TiO_2 systems (Table 2). They were identified as $C_6H_5N_3O$ (product A; *m*/*z* 136.0505), $C_6H_5N_3O_2$ (product B; *m*/*z* 152.0454), $C_6H_5N_3O_3$ (product C; *m*/*z* 168.0404), $C_5H_5N_3O_4$ (product D; *m*/*z* 172.0353), $C_4H_3N_3O_4$ (product E; *m*/*z* 158.0196), $C_6H_3N_3O_2$ (product F; *m*/*z* 150.0298), $C_4H_3N_3O_2$ (product G; *m*/*z* 126.0298) and $C_4H_3N_3O_3$ (product H; *m*/*z* 142.0247). Some of these products were also reported in other studies.[12,25]

Based on the relative intensity variations of these products (Table 2 and Fig. S2†), the main reaction pathways may involve a series of additions, substitutions and cleavages of the phenyl structure induced by $^{\cdot}OH$ (Fig. 2), resulting in the transformation from 1H-BTA to product E or H. Another pathway also involves oxidation and cleavage of the phenyl structure, with a pathway from 1H-BTA to product G. These proposed pathways were verified by the observed variation tendencies (Table 2). Products A and E had higher abundances than the other products. Product A has a mass of 136.0505 Da ($[M + H]^+$), which differs from $[1H\text{-}BTA + H]^+$ with a ~16 Da moiety (supposed to be a hydroxyl). It is the simplest product oxidized from 1H-BTA under $^{\cdot}OH$ attack with a high abundance during the initial stage of the reaction. Product E ($[M + H]^+$; 158.0196 Da) has an open structure with two excessively oxidized carboxylic moieties, and its stability contributed to the accumulation in the later stage of the reaction. Other products are probably not stable and tend to be further oxidized; their relative intensity decreased in the later stage of a 60 min reaction.

Similar products were identified in the UV/TiO_2 system with the slight difference that product F was generated. A pathway from 1H-BTA to product F and another pathway from 1H-BTA to product E or product H were proposed (Fig. 2). This difference may be due to the different active radical species in these two treatments. In UV/TiO_2, a superoxide radical ($^{\cdot}O_2^-$) can be generated, which induces a continuous oxidation to form product F. The proposed reaction mechanism has been reported in a study investigating the oxidation of 1H-BTA using ozone.[9] Variation tendencies of these products (Table 2 and Fig. S2b†) supported our proposed degradation pathways. Even though products A and E were also stable with high abundances, their peak times were delayed, indicating decreased reaction rates. Some of these products have been found in aerobic biological degradation,[26] and the release of these products into receiving waters may induce assimilation and phytotransformation in aquatic vegetation.[27] Therefore, these transformation products in both systems may have potential risks to the environment and organisms, but the actual biological effects remain unknown.

3.4. Response of differently expressed protein networks to degradation products

The reaction time of 1H-BTA samples for proteomics analysis was selected based on the variation tendencies of degradation products in both systems (Table 2). At 30 min, the abundance of product E was relatively high in the UV/H_2O_2 system, while product A was predominant in the UV/TiO_2 systems. Thus, the toxicities of these two dominant products can be compared.

Compared to the *E. coli* exposed to untreated 1H-BTA, the cells exposed to the UV/H_2O_2 degradation product mixture expressed 152 up-regulated and 140 down-regulated proteins (Table S4†). Based on the protein network (http://string-db.org/) and KEGG metabolism pathway analyses, the up-regulated proteins were enriched in the networks related to ribosome, transporter, and carbon metabolism. (Fig. 3 and Table S5†), suggesting that the *E. coli* exposed to the UV/H_2O_2 degradation product mixture had higher metabolism activity than that exposed to 1H-BTA. It also means that 1H-BTA may be detoxified after UV/H_2O_2 treatment.

Key node proteins enriched in the above-mentioned protein network and metabolism pathways are summarized in Fig. 4. It should be noted that some of these proteins catalyzed the conversion between carbohydrates and pyruvate (Table S5†). In this process, the produced ribose would be used for the syntheses of nucleotides, nucleic acids, DNA and RNA. Another important intermediate, 4-phosphate-erythrose, was the precursor for the biosynthesis of aromatic amino acids. Therefore, the up-regulation of this pathway indicated increased syntheses of DNA, RNA, ATP and amino acids.

In ribosomes, the up-regulation of key proteins in small and large ribosomal subunits enhanced the biosynthesis efficiency of proteins. Various amino acids for protein syntheses were generated in up-regulated alanine, aspartate and glutamate metabolism pathways and amino acid biosynthesis pathways, resulting in a series of up-regulated proteins in *E. coli* exposed to the UV/H_2O_2 degradation product mixture compared to 1H-BTA. To provide precursors and energy for these up-regulated pathways, the up-expression of proteins in the pyruvate metabolism pathway accelerated the tricarboxylic acid cycle for the generation of NADH, amino acids and other organic acids. Furthermore, the transformations of GTP and ATP in the purine metabolism pathway were also enhanced.

The down-regulated proteins enriched in the carbon metabolism and glycolysis/gluconeogenesis pathways primarily decreased the conversion between β-D-fructose-6P and β-D-fructose-1,6P, and the transformation between glycerate-2P and phosphoenol-pyruvate (Fig. S3†). However, all these down-regulated reactions had bypasses. As the up-regulated proteins mentioned above could catalyze other bypasses, these down-regulated proteins would not inhibit the cellular metabolism. Therefore, the 30 min UV/H_2O_2 degradation products (*e.g.*, product E) would be safe for *E. coli* at pathway and network levels.

A similar network with 137 up-regulated proteins (Tables S4 and S5†) in the *E. coli* exposed to the UV/TiO_2 degradation product mixture was observed (Fig. S4†). Compared to UV/H_2O_2, fewer proteins were enriched in the ribosome network, and it was consistent with the down expression of some proteins enriched in aminoacyl-tRNA biosynthesis for protein

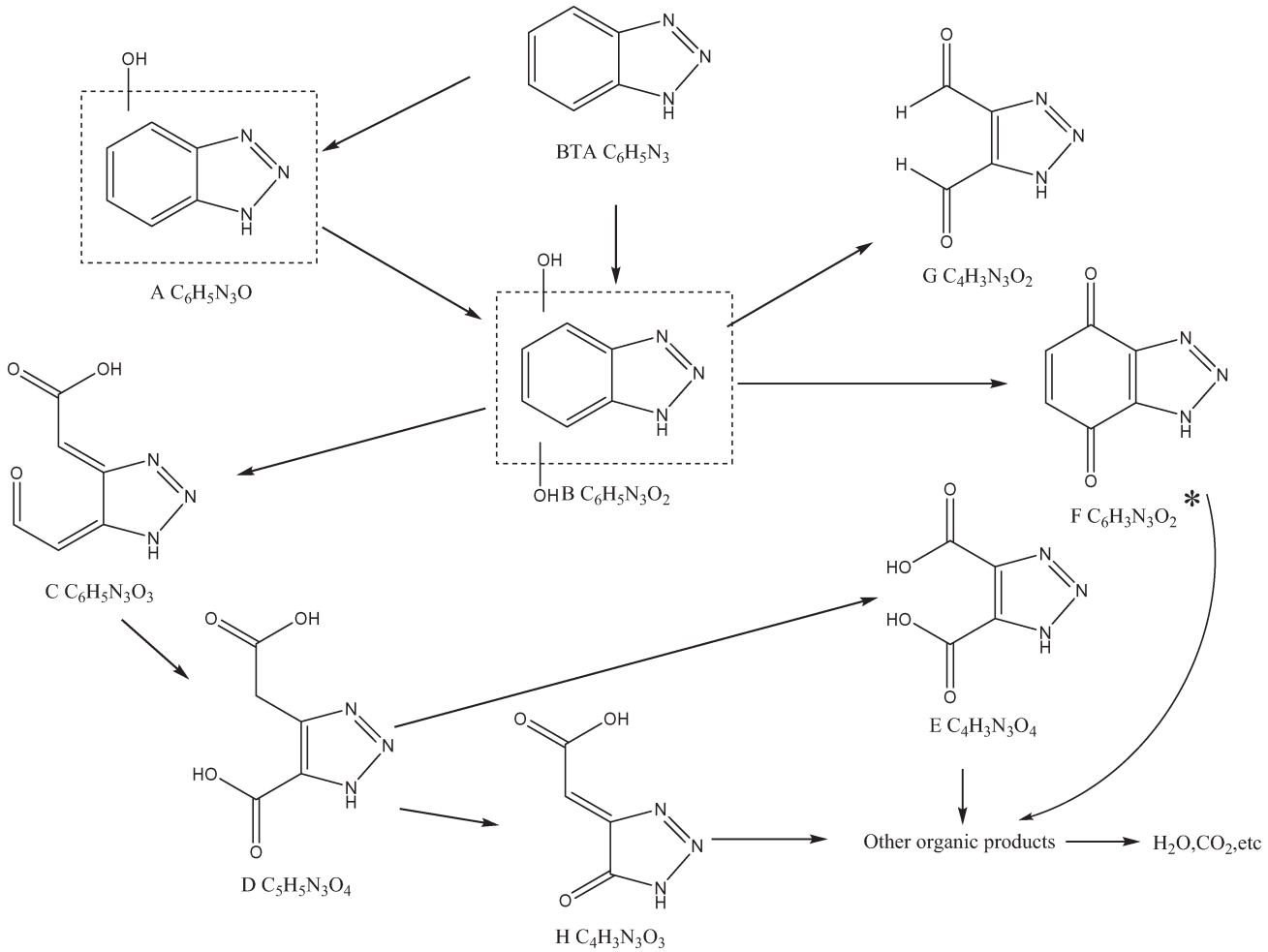

Fig. 2 Proposed generative pathways of products in UV/H_2O_2 and UV/TiO_2 treatments.

synthesis. These findings verified that the UV/TiO_2 degradation products (*e.g.*, product A) inhibited the biosynthesis of some proteins.

On the other hand, the down expression of rplI, rplQ, rplT, rpmA, rpmE, rpsE, rpsG, rpsM and rpsN (Fig. S5†) enriched in ribosomes for protein synthesis revealed that the UV/TiO_2 degradation products (*e.g.*, product A) still somewhat inhibited the protein networks of *E. coli*. Overall, the abundant product A generated in UV/TiO_2 treatment was more toxic than the abundant product E in UV/H_2O_2, suggesting that the degradation degree of 1H-BTA had an impact on the residual toxicities of the products.

3.5. Influencing factors

Degradation of 1H-BTA with different experimental conditions was explored (Fig. 5). For UV/H_2O_2, the k_{app} decreased from 2.01×10^{-3} s^{-1} to 1.37×10^{-3} s^{-1} when the solution pH value increased from 3.0 to 11.0 (Fig. 5a). The redox potentials of $^{\cdot}OH/H_2O$ at pH 3.0, 5.0, 7.0, 9.0 and 11.0 are 2.62, 2.51, 2.39, 2.29 and 2.15 V, respectively,[28] resulting in a decreasing reaction rate of 1H-BTA. Compared to UV/H_2O_2, the pH variation had more significant impacts on the degradation efficiency in UV/TiO_2 (Fig. 5b). The reaction at pH = 7.0 had the highest efficiency with a k_{app} of 1.87×10^{-3} s^{-1}. Under strong acidic and alkaline conditions, the k_{app} decreased rapidly. These results suggested that strong acidic and alkaline conditions should be avoided in the degradation of 1H-BTA using UV/TiO_2. In normal water treatment processes, especially drinking water treatment, the pH value is usually maintained at neutral conditions. Besides, considering that the operation of UV/H_2O_2 is more simple than UV/TiO_2, these results suggested that UV/H_2O_2 would be more advantageous for contaminant removal in actual water treatment.

Effects of typical photocatalysis inhibitors, *e.g.*, humic acid, NO_3^- and Cl^-, were also explored. As the humic acid concentration increased from 0 mg L^{-1} to 200 mg L^{-1}, the k_{app} in UV/H_2O_2 decreased from 1.63×10^{-3} s^{-1} to 0.22×10^{-3} s^{-1}. For UV/TiO_2, the impact of humic acid (200 mg L^{-1}) was severe with a k_{app} of 0.01×10^{-3} s^{-1}, which was approximately 200 times lower than 1.87×10^{-3} s^{-1} in the control group. Humic acid can consume $^{\cdot}OH$, and it can occupy surface active sites of TiO_2 and poison catalysts. Similar inhibition effects were also observed previously.[28–30]

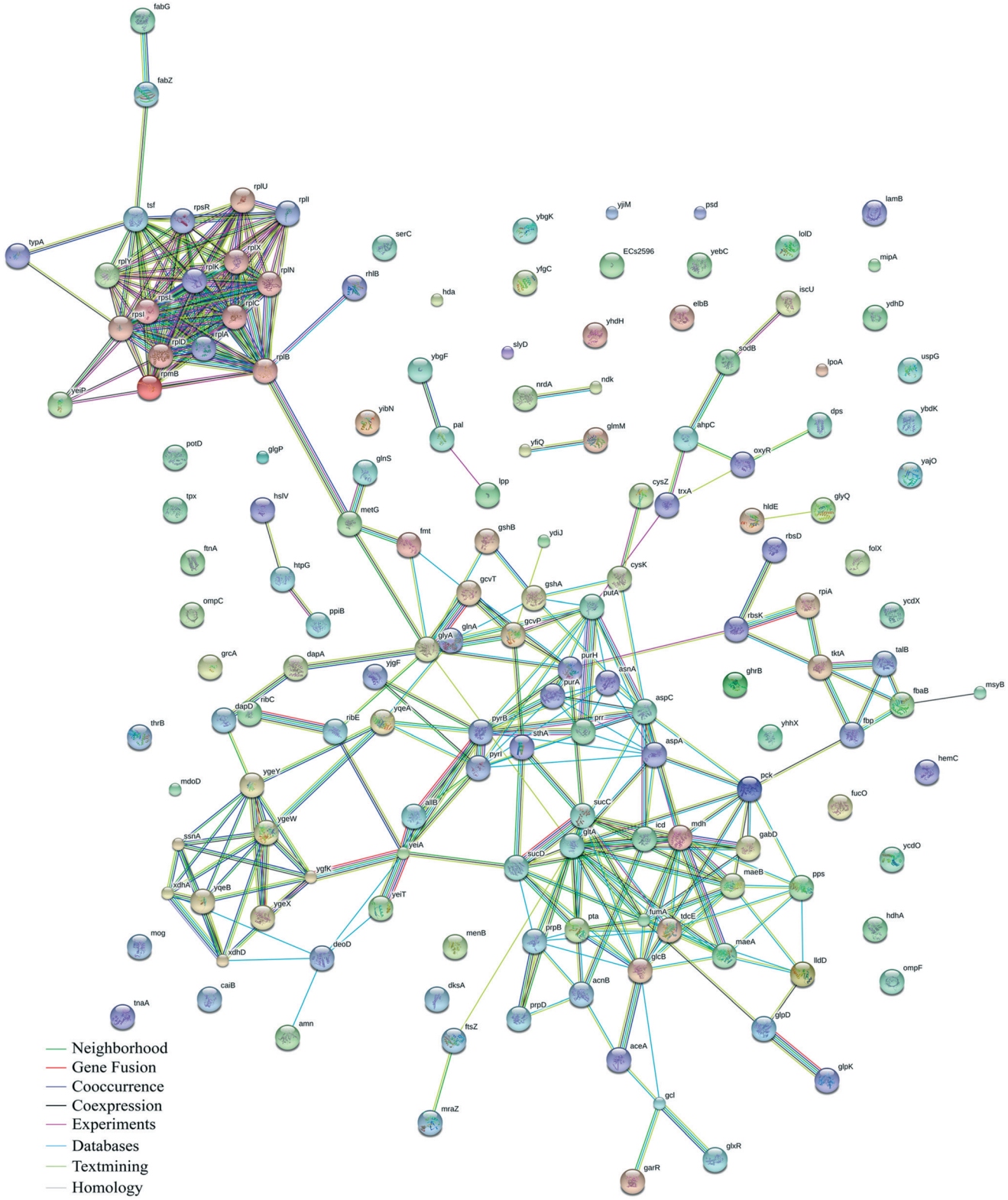

Fig. 3 Biological networks of up-regulated expressed proteins in *E. coli* after the exposure to the degradation products in UV/H_2O_2 treatment compared to untreated 1H-BTA.

As the ε of NO_3^- and Cl^- at 280 nm is 139 ± 41 M^{-1} cm^{-1} and 252 ± 28 M^{-1} cm^{-1} (Table S3†), their UV screening effect can be neglected. The k_{app} gradually decreased with increasing concentration of NO_3^- (Fig. 5e and f). A high concentration of NO_3^- (>10 mg L^{-1}) screened and reduced the penetration of UV irradiation.[31] In contrast, Cl^- had different effects on the UV/H_2O_2 and UV/TiO_2 systems (Fig. 5g and h). A slight variation was observed as the Cl^- concentration increased

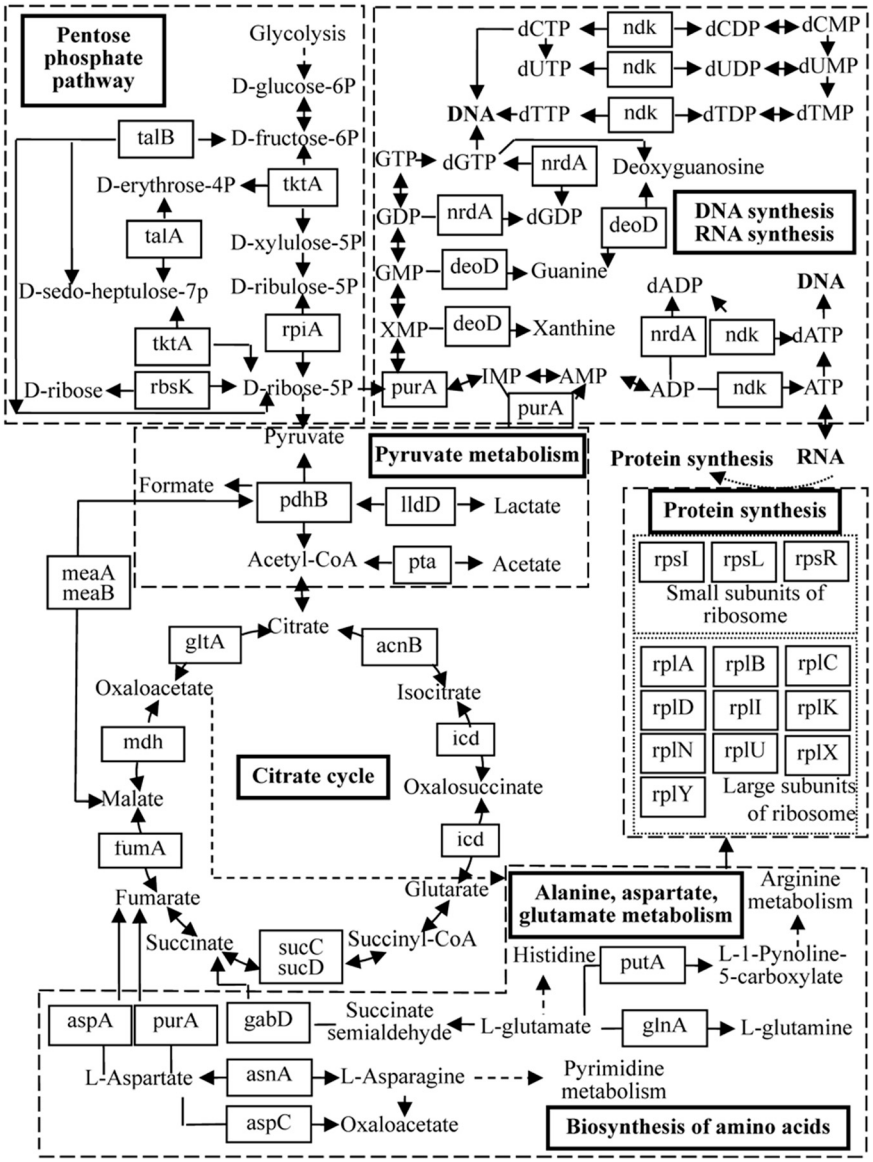

Fig. 4 Metabolic networks of up-regulated expressed proteins in *E. coli* after the exposure to the degradation products in UV/H_2O_2 treatment compared to untreated 1H-BTA.

from 0 to 500 mg L^{-1} in the UV/H_2O_2 system. The reaction between Cl^- and $^{\bullet}OH$ follows:[28]

$$^{\bullet}OH + Cl^- \rightarrow {}^{\bullet}ClOH^- \quad (k = 4.3 \times 10^9\ M^{-1}\ s^{-1}) \tag{3}$$

$$^{\bullet}ClOH^- \rightarrow {}^{\bullet}OH + Cl^- \quad (k = 6.0 \times 10^9\ M^{-1}\ s^{-1}) \tag{4}$$

These reactions were reversible at neutral conditions, which may have little effect on the $^{\bullet}OH$ reaction. For UV/TiO_2, the k_{app} decreased from 1.87×10^{-3} s^{-1} (control) to 0.91×10^{-3} s^{-1} (500 mg L^{-1} Cl^-), and the inhibition mechanism may involve the scavenging of active holes on TiO_2:

$$Cl^- + h^+ \rightarrow Cl^{\bullet} \tag{5}$$

The adsorption of Cl^- onto the TiO_2 surface reduced the $^{\bullet}OH$ yield.

3.6. Degradation of 1*H*-benzotriazole in an actual water matrix and cost evaluation

In the UV/H_2O_2 system, k_{app} decreased from 1.63×10^{-3} s^{-1} to 0.63×10^{-3} s^{-1} and 0.79×10^{-3} s^{-1} with two source water matrixes, but for two finished water matrices, only slight inhibitions were observed (Fig. 6). In the UV/TiO_2 system, the inhibition was more significant; *e.g.*, k_{app} decreased from 1.87×10^{-3} s^{-1} to 0.92×10^{-3} s^{-1} and 0.68×10^{-3} s^{-1} with two finished waters. This result reconfirmed that the UV/H_2O_2 system is more robust than UV/TiO_2 for the degradation of 1H-BTA in actual drinking water treatment. Two source waters contained more NOM (TOC), aromatic organic matter (UV_{254}) and anions (Cl^-, SO_4^{2-} and NO_3^-) than finished waters (Table S6†). Thus, these impurities in the source waters induced a more significant impact on 1H-BTA degradation. Determination of the amounts of organic matter and anions in an actual water matrix and the

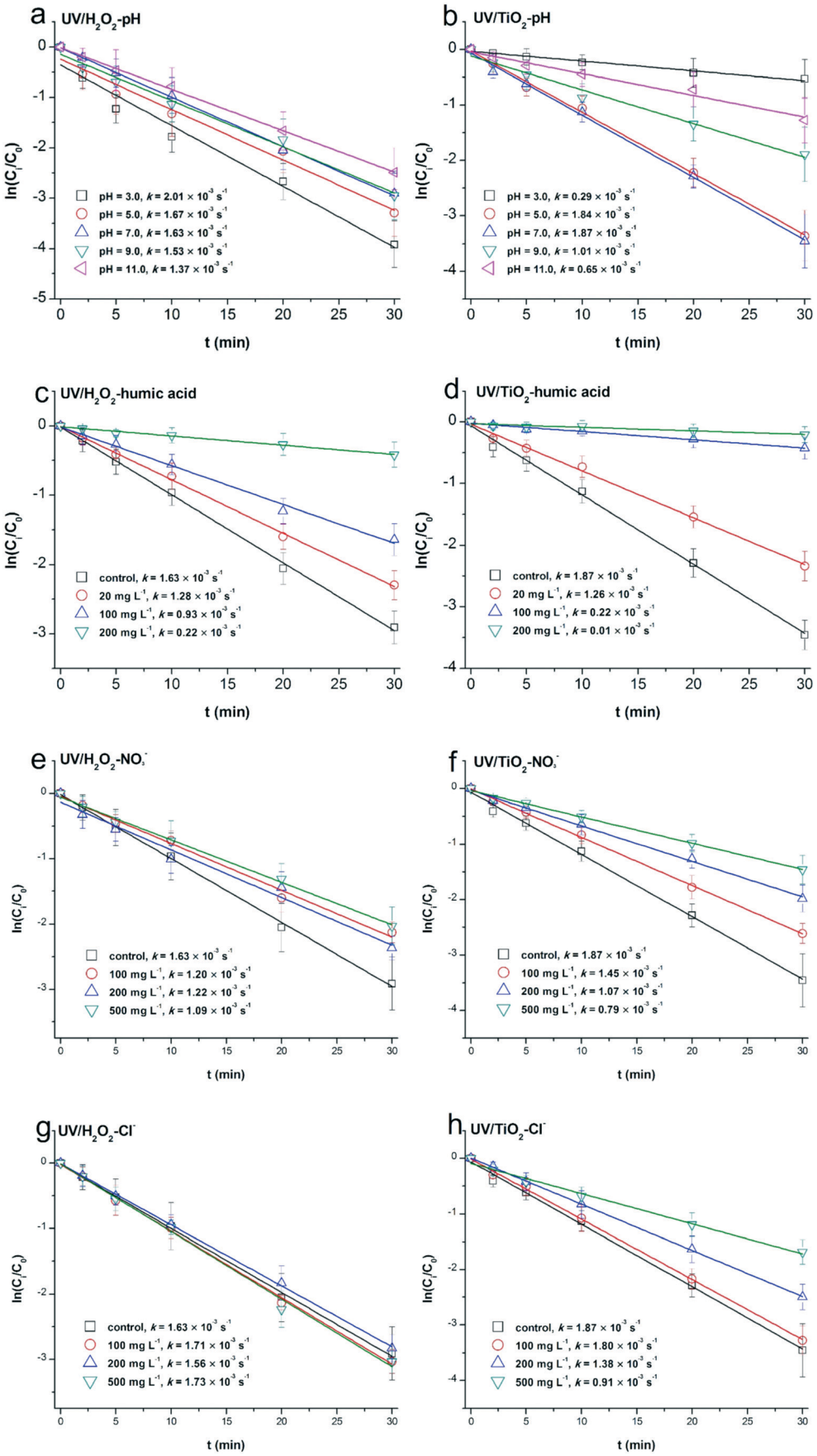

Fig. 5 Role of water quality parameters on the degradation kinetics of 1H-BTA.

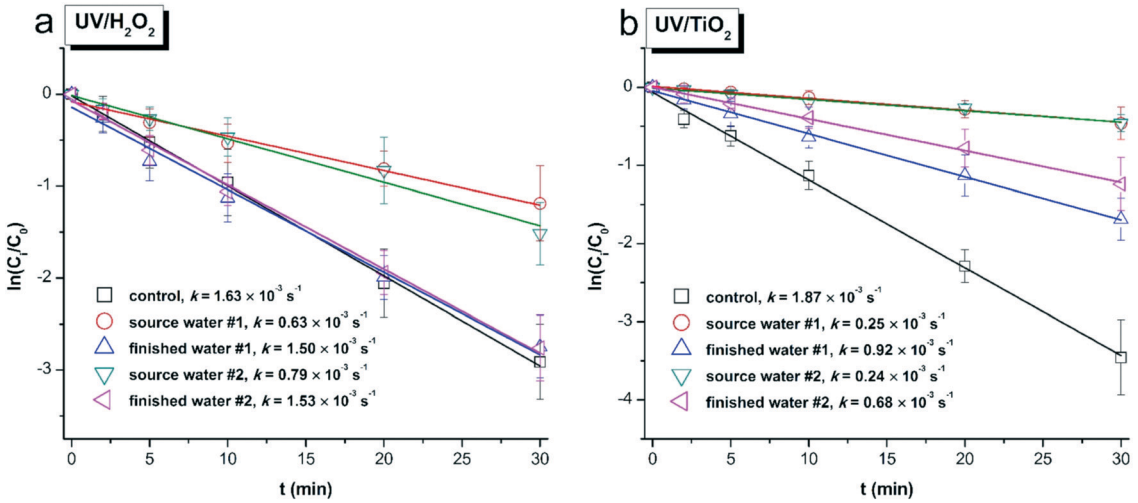

Fig. 6 Variation tendencies of 1H-BTA in natural source water and finished water.

further quantification of their impacts are important issues for the successful application of UV-AOPs.

The electrical energy per order (EE/O) value was used to evaluate the electrical cost. The EE/O is defined as the electrical energy in kilowatt hours (kW h) required to degrade a specific contaminant by one order of magnitude in 1 m^3 contaminated water. Generally, EE/O can be calculated:[32]

$$\mathrm{EE/O} = \frac{P \times t}{V \times \lg\left(c_i / c_f\right)} \quad (6)$$

wherein, EE/O has the unit of kW h m^{-3} $order^{-1}$; P is the total electrical power to drive UV irradiation entering the reactor, kW; t is the time in which 90% of 1H-BTA is removed, h; V indicates the volume of the given reaction system, m^3; c_i is the initial concentration of the targeted contaminant, mg L^{-1}; c_f is the final concentration of the targeted contaminant, mg L^{-1}. The EE/O values were calculated to be 0.0365 kW h m^{-3} $order^{-1}$ and 0.0319 kW h m^{-3} $order^{-1}$ in the control UV/H_2O_2 and UV/TiO_2 systems, respectively (Table S7†).

Variations of EE/O values highly depend on the k_{app}. In the UV/H_2O_2 system, the EE/O value reached 0.0641 kW h m^{-3} $order^{-1}$ with 100 mg L^{-1} humic acid, and it increased to 0.0955 kW h m^{-3} $order^{-1}$ with source water #1, indicating an increased cost for source water treatment. In the UV/TiO_2 system, the EE/O value significantly increased at pH = 3.0, pH = 11.0 or with the addition of humic acid. The EE/O values increased to 0.2341 kW h m^{-3} $order^{-1}$ and 0.2453 kW h m^{-3} $order^{-1}$, respectively, when using source water matrixes #1 and #2, suggesting that the occurrence of natural impurities will significantly increase the electrical cost for 1H-BTA degradation in UV/TiO_2 treatment.

4. Conclusion

Degradation of 1H-BTA followed pseudo-first order degradation kinetics with k_{app} of 1.63×10^{-3} s^{-1} ($t_{0.5}$ at 7.09 min) and 1.87×10^{-3} s^{-1} ($t_{0.5}$ at 6.18 min), respectively, in low power 280 nm UV/H_2O_2 and UV/TiO_2 systems, and radical oxidation was the dominant reaction mechanism. In these two systems, $k_{\cdot OH\text{-}BTA}$ was calculated to be $(7.1 \pm 0.8) \times 10^9$ M^{-1} s^{-1} and $(6.9 \pm 0.7) \times 10^9$ M^{-1} s^{-1}. Generation of low-level oxidative intermediates (*e.g.* $C_6H_5N_3O$) occurred at the early stage of the reaction. In contrast, further oxidative intermediates (*e.g.* $C_4H_3N_3O_4$) were observed at the later stage. Based on the proteomics analysis, the significant activation of ribosome, transporter and tricarboxylic acid cycle metabolisms in *E. coli*, which exposed to the later degradation product mixture, suggested that the toxicity of 1H-BTA may be weakened. In conclusion, incomplete mineralization using hydroxyl radical oxidation likewise has potential for the degradation and detoxification of 1H-BTA.

Conflicts of interest

The authors declared that they have no conflicts of interest to this work.

Acknowledgements

This project was supported by the National Natural Science Foundation of China (No. 51778270), the Science and Technology Planning Project of Guangdong Province, China (Grant No. 2014A020216014) and the Fundamental Research Funds for the Central Universities of China (No. 21617448).

References

1 H. Nakata, S. Murata and J. Filatreau, Occurrence and concentrations of benzotriazole UV stabilizers in marine organisms and sediments from the Ariake Sea, Japan, *Environ. Sci. Technol.*, 2015, **4**, 688–710.

2 H. Nagayoshi, K. Kakimoto, S. Takagi, Y. Konishi, K. Kajimura and T. Matsuda, Benzotriazole ultraviolet stabilizers show potent activities as human aryl hydrocarbon receptor ligands, *Environ. Sci. Technol.*, 2015, **49**, 578–587.

3 A. G. Asimakopoulos, L. Wang, N. S. Thomaidis and K. Kannan, Benzotriazoles and benzothiazoles in human urine from several countries: a perspective on occurrence, biotransformation, and human exposure, *Environ. Int.*, 2013, **59**, 274–281.

4 S. Weiss, J. Jakobs and T. Reemtsma, Discharge of three benzotriazole corrosion inhibitors with municipal wastewater and improvements by membrane bioreactor treatment and ozonation, *Environ. Sci. Technol.*, 2006, **40**, 7193–7199.

5 H. Janna, M. D. Scrimshaw, R. J. Williams, J. Churchley and J. P. Sumpter, From Dishwasher to Tap? Xenobiotic Substances Benzotriazole and Tolyltriazole in the Environment, *Environ. Sci. Technol.*, 2011, **45**, 3858–3864.

6 G. H. LeFevre, A. Lipsky, K. C. Hyland, A. C. Blaine, C. P. Higgins and R. G. Luthy, Benzotriazole (BT) and BT plant metabolites in crops irrigated with recycled water, *Environ. Sci.: Water Res. Technol.*, 2017, **3**, 213–223.

7 F. Busetti, M. Ruff and K. L. Linge, Target screening of chemicals of concern in recycled water, *Environ. Sci.: Water Res. Technol.*, 2015, **1**, 659–667.

8 D. Voutsa, P. Hartmann, C. Schaffner and W. Giger, Benzotriazoles, alkylphenols and bisphenol a in municipal wastewaters and in the Glatt River, Switzerland, *Environ. Sci. Pollut. Res.*, 2006, **13**, 333–341.

9 D. B. Mawhinney, B. J. Vanderford and S. A. Snyder, Transformation of 1H-benzotriazole by ozone in aqueous solution, *Environ. Sci. Technol.*, 2012, **46**, 7102–7111.

10 J. Xu, L. Li, C. Guo, Y. Zhang and S. Wang, Removal of benzotriazole from solution by BiOBr photocatalysis under simulated solar irradiation, *Chem. Eng. J.*, 2013, **221**, 230–237.

11 D. K. Kim, Y. He, J. Jeon and K. E. O'Shea, Irradiation of ultrasound to 5-methylbenzotriazole in aqueous phase: Degradation kinetics and mechanisms, *Ultrason. Sonochem.*, 2016, **31**, 227–236.

12 E. Borowska, E. Felis and J. Kalka, Oxidation of benzotriazole and benzothiazole in photochemical processes: Kinetics and formation of transformation products, *Chem. Eng. J.*, 2016, **304**, 852–863.

13 N. K. V. Leitner and B. Roshani, Kinetic of benzotriazole oxidation by ozone and hydroxyl radical, *Water Res.*, 2010, **44**, 2058–2066.

14 N. D. L. Cruz, L. Esquius, D. Grandjean, A. Magnet, A. Tungler, L. F. D. Alencastro and C. Pulgarín, Degradation of emergent contaminants by UV, UV/H_2O_2 and neutral photo-Fenton at pilot scale in a domestic wastewater treatment plant, *Water Res.*, 2013, **47**, 5836–5845.

15 Y. Ding, C. Yang, L. Zhu and J. Zhang, Photoelectrochemical activity of liquid phase deposited TiO_2 film for degradation of benzotriazole, *J. Hazard. Mater.*, 2010, **175**, 96–103.

16 M. C. Dodd, H.-P. E. Kohler and U. Von Gunten, Oxidation of antibacterial compounds by ozone and hydroxyl radical: Elimination of biological activity during aqueous ozonation processes, *Environ. Sci. Technol.*, 2009, **43**, 2498–2504.

17 D. A. Pillard, J. S. Cornell, D. L. Dufresne and M. T. Hernandez, Toxicity of benzotriazole and benzotriazole derivatives to three aquatic species, *Water Res.*, 2001, **35**, 557–560.

18 H. S. Ou, J. S. Ye, S. Ma, C. H. Wei, N. Y. Gao and J. Z. He, Degradation of ciprofloxacin by UV and UV/H_2O_2 via multiple-wavelength ultraviolet light-emitting diodes: Effectiveness, intermediates and antibacterial activity, *Chem. Eng. J.*, 2016, **289**, 391–401.

19 C. Duca, G. Imoberdorf and M. Mohseni, Effects of inorganics on the degradation of micropollutants with vacuum UV (VUV) advanced oxidation, *J. Environ. Sci. Health, Part A: Toxic/Hazard. Subst. Environ. Eng.*, 2017, **52**, 524–532.

20 O. S. Keen and K. G. Linden, Degradation of antibiotic activity during UV/H_2O_2 advanced oxidation and photolysis in wastewater effluent, *Environ. Sci. Technol.*, 2013, **47**, 13020–13030.

21 M. M. Huber, S. Canonica, G. Y. Park and U. Von Gunten, Oxidation of pharmaceuticals during ozonation and advanced oxidation processes, *Environ. Sci. Technol.*, 2003, **37**, 1016–1024.

22 E. L. Schymanski, J. Jeon, R. Gulde, K. Fenner, M. Ruff, H. P. Singer and J. Hollender, Identifying Small Molecules via High Resolution Mass Spectrometry: Communicating Confidence, *Environ. Sci. Technol.*, 2014, **48**, 2097–2098.

23 H. S. Ou, J. Liu, J. S. Ye, L. L. Wang, N. Y. Gao and J. Ke, Degradation of tris(2-chloroethyl) phosphate by ultraviolet-persulfate: Kinetics, pathway and intermediate impact on proteome of *Escherichia coli*, *Chem. Eng. J.*, 2016, **308**, 386–395.

24 E. Sieswerda, R. L. Mulder, I. W. E. M. V. Dijk, E. C. V. Dalen, S. L. Knijnenburg, H. J. H. V. D. Pal, M. S. Mud, R. C. Heinen, H. N. Caron and L. C. M. Kremer, Theoretical study of benzotriazole UV photostability: ultrafast deactivation through coupled proton and electron transfer triggered by a charge-transfer state, *J. Am. Chem. Soc.*, 2004, **126**, 2912–2922.

25 A. Müller, S. C. Weiss, J. Beißwenger, H. G. Leukhardt, W. Schulz, W. Seitz, W. K. L. Ruck and W. H. Weber, Identification of ozonation by-products of 4- and 5-methyl-1H-benzotriazole during the treatment of surface water to drinking water, *Water Res.*, 2012, **46**, 679–690.

26 S. Huntscha, T. B. Hofstetter, E. L. Schymanski, S. Spahr and J. Hollender, Biotransformation of Benzotriazoles: Insights from Transformation Product Identification and Compound-Specific Isotope Analysis, *Environ. Sci. Technol.*, 2014, **48**, 4435–4443.

27 G. H. LeFevre, C. E. Muller, R. J. X. Lo, R. G. Luthy and E. S. Sattely, Rapid Phytotransformation of Benzotriazole Generates Synthetic Tryptophan and Auxin Analogs in Arabidopsis, *Environ. Sci. Technol.*, 2015, **49**, 10959–10968.

28 Y. Xiao, L. Zhang, Z. Wei, K. Y. Lim, R. D. Webster and T. T. Lim, Comparative evaluation of iodoacids removal by UV/persulfate and UV/H_2O_2 processes, *Water Res.*, 2016, **102**, 629–639.

29 Q. N. Liao, F. Ji, J. C. Li, X. Zhan and Z. H. Hu, Decomposition and mineralization of sulfaquinoxaline sodium during UV/H_2O_2 oxidation processes, *Chem. Eng. J.*, 2016, **284**, 494–502.

30 J. Sharma, I. M. Mishra and V. Kumar, Degradation and mineralization of Bisphenol A (BPA) in aqueous solution using advanced oxidation processes: UV/H_2O_2 and UV/$S_2O_8^{2-}$ oxidation systems, *J. Environ. Manage.*, 2015, **156**, 266–275.

31 C. Y. Wang, L. Y. Zhu, M. C. Wei, P. Chen and G. Q. Shan, Photolytic reaction mechanism and impacts of coexisting substances on photodegradation of bisphenol A by Bi_2WO_6 in water, *Water Res.*, 2012, **46**, 845–853.

32 X. He, A. A. D. L. Cruz and D. D. Dionysiou, Destruction of cyanobacterial toxin cylindrospermopsin by hydroxyl radicals and sulfate radicals using UV-254 nm activation of hydrogen peroxide, persulfate and peroxymonosulfate, *J. Photochem. Photobiol., A*, 2013, **251**, 160–166.

